MDPI

Article

Influence of Different Salts on the G-Quadruplex Structure Formed from the Reversed Human Telomeric DNA Sequence

Lydia Olejko †, Anushree Dutta †, Kosar Shahsavar ‡ and Ilko Bald *

Institute of Chemistry–Hybrid Nanostructures, University of Potsdam, 14476 Potsdam, Germany

* Correspondence: bald@uni-potsdam.de
† These authors contributed equally to this work.
‡ Permanent address: Department of Life Science Engineering, Faculty of New Sciences & Technologies, University of Tehran, Tehran 999067, Iran.

Abstract: G-rich telomeric DNA plays a major role in the stabilization of chromosomes and can fold into a plethora of different G-quadruplex structures in the presence of mono- and divalent cations. The reversed human telomeric DNA sequence (5′-(GGG ATT)$_4$; RevHumTel) was previously shown to have interesting properties that can be exploited for chemical sensing and as a chemical switch in DNA nanotechnology. Here, we analyze the specific G-quadruplex structures formed by RevHumTel in the presence of K$^+$, Na$^+$, Mg^{2+} and Ca^{2+} cations using circular dichroism spectroscopy (CDS) and Förster resonance energy transfer (FRET) based on fluorescence lifetimes. CDS is able to reveal strand and loop orientations, whereas FRET gives information about the distances between the 5′-end and the 3′-end, and also, the number of G-quadruplex species formed. Based on this combined information we derived specific G-quadruplex structures formed from RevHumTel, i.e., a chair-type and a hybrid-type G-quadruplex structure formed in presence of K$^+$, whereas Na$^+$ induces the formation of up to three different G-quadruplexes (a basket-type, a propeller-type and a hybrid-type structure). In the presence of Mg^{2+} and Ca^{2+} two different parallel G-quadruplexes are formed (one of which is a propeller-type structure). This study will support the fundamental understanding of the G-quadruplex formation in different environments and a rational design of G-quadruplex-based applications in sensing and nanotechnology.

Keywords: guanine quadruplexes; förster resonance energy transfer (FRET); circular dichroism; DNA nanotechnology

1. Introduction

Apart from the well-known double helix structure, DNA can also adopt fascinating higher order structures such as guanine (G) quadruplex or i-motif structures [1–4]. Guanine-rich DNA sequences, usually found in telomeres (located at the end of euka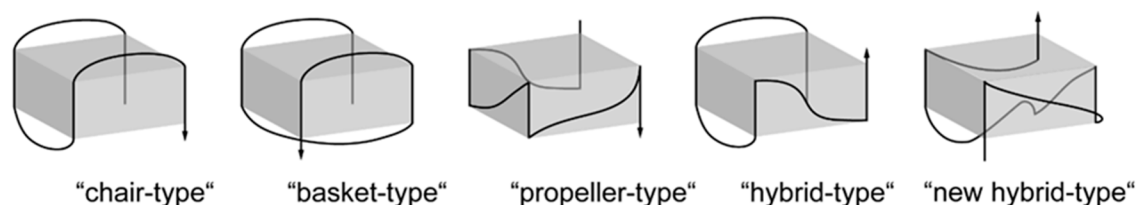ryotic chromosomes) [5,6], tend to fold in the presence of metal ions to form secondary structures of two or more G-tetrads termed as G-quadruplex. The G-tetrad plane consists of four associated G bases stabilized by eight Hoogsteen hydrogen bonds and a cation in the middle of the G-tetrad (see Scheme 1A) [4,7–9]. The metal cation coordination to the four central oxygen atoms of the G bases weakens the electronic repulsion between the oxygen atoms resulting in stronger hydrogen bonds and therefore stabilization of the G-tetrad [10]. Based on the number of DNA strands (four, two and one) involved in the folding, G-quadruplexes can be classified into tetramolecular, bimolecular or intermolecular and unimolecular or intramolecular, respectively. Similarly, depending on the DNA strand orientation, the G-quadruplex structure can be divided into anti-parallel (opposite strand orientations) and parallel (same strand orientation) structures (see Figure 1B) [4,9–11]. The G-tetrads can be connected with lateral and diagonal loops leading to so-called "basket-type" or "chair-type" G-quadruplexes (anti-parallel) or with external loops leading to "propeller-type"

G-quadruplexes (parallel) (see Scheme 1B). A combination of lateral and/or diagonal loops with external loops lead to "hybrid-type" G-quadruplexes (combination of anti-parallel and parallel, Figure 1B) [4,9,10]. Therefore, based on different loop and strand orientations, the distance between 5′- and 3′-end will differ in the G-quadruplex structure varying from 4 nm to 6 nm, as schematically depicted in Scheme 1B,C. Herein, the distances between 5′- and 3′-end in the folded structure have been calculated based on the X-ray crystallography, NMR and molecular dynamics data reported in literature for the human telomeric DNA [12,13].
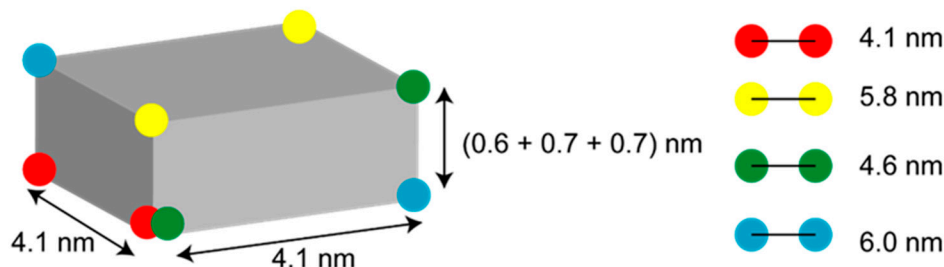

Scheme 1. Structural basics of G-quadruplexes. (**A**) G-quadruplexes are stacked G-tetrads which are four-associated guanine bases stabilized by hydrogen bonds and a cation in the middle. (**B**) The G-quadruplex structures can be divided according to their strand polarities and loop orientation. G-quadruplexes can, for example, fold into anti-parallel ("chair-type" and "basket-type") or into parallel ("propeller-type") structures. A combination of both leads to "hybrid-type" G-quadruplexes. The 3′-end is illustrated with an arrow. (**C**) Due to different strand routings the 5′- and 3′-end of the DNA are at different distances depending on the orientation to each other. A linker length of 0.7 nm between fluorophore and DNA has been taken into account for the calculation between green and blue dots.
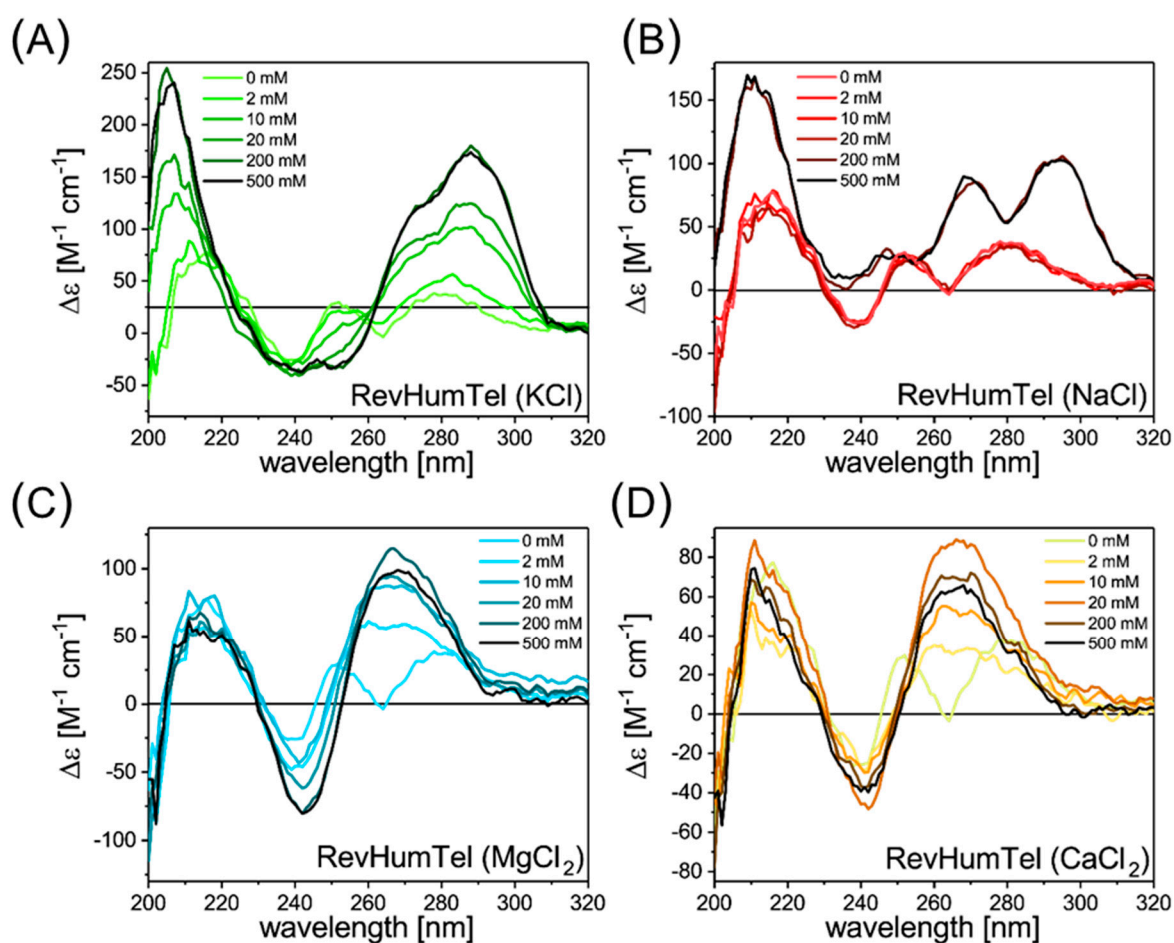
Figure 1. CD spectra of RevHumTel (c = 8.6 μM) in presence of different salts showing the structural polymorphism. (**A**) The CD spectra after KCl addition gives rise to a positive peak at 288 nm with a shoulder at 275 nm and a negative peak at (240-250) nm. These CD spectra indicate the formation of a "hybrid-type" G-quadruplex structure. (**B**) Two positive bands at 270 nm and 290 nm and a minimum at 235 nm appear in presence of NaCl. The CD spectra can be attributed to the formation of a "hybrid-type" or a mixture of parallel and anti-parallel G-quadruplexes. (C,D) CD spectra in presence of $MgCl_2$ (**C**) and $CaCl_2$ (**D**). The CD spectra in presence of these divalent cations have a similar shape. Both give rise to a positive peak at (240-245) nm and a negative peak at 265 nm. These CD spectra can be ascribed to the formation of a parallel G-quadruplex structure.

CD spectroscopy, which is based on the effect that chiral (optically active) molecules absorb right- and left-handed circularly polarized light differently and can be used for structural investigations of biomolecules such as DNA [14]. The same has been extended to determine the specific structure of G-quadruplexes using circular dichroism (CD) spectroscopy [15,16]. In this sense, it can also be used to analyze the different structures of certain G-quadruplexes which ideally should lead to different CD spectra. This effect is ascribed to the varying stacking interactions due to different glycosidic angles and strand orientations [17,18]. For example, a parallel G-quadruplex structure should give rise to a positive peak at (260–265) nm and a negative peak at 240 nm. Positive peaks at (290–295) nm and (240–250) nm and a negative peak at (240–275) nm are a sign of the formation of anti-parallel G-quadruplex structures. On the other hand, hybrid-type G-quadruplex structures lead to a positive peak at 290 nm with a shoulder at (260–270) nm and a negative peak at 240 nm [15,16,19–23].

From the human telomeric DNA (HumTel, (TTA GGG)$_n$), it is known that environmental conditions have a great influence on the overall G-quadruplex structure (see also supporting information (SI), Figure S1). Many studies revealed that a variety of changes

both within the DNA sequence and external conditions influence the formation of specific G-quadruplex structures [24,25]. The G-quadruplex structure is different for telomeric DNA and telomeric RNA [26], it is altered by changing the number of flanking nucleotides (AG_3 (T_2AG_3)$_3$, TAG_3 (T_2AG_3)$_3$, TAG_3 (T_2AG_3)$_3T_2$ and A_3G_3 (T_2AG_3)$_3A_2$) [27,28], the number of involved repeating units ((TTA GGG)$_2$ vs. (TTA GGG)$_4$) [29,30] or the strand polarization (HumTel: (TTA GGG)$_4$ vs. RevHumTel: (GGG ATT)$_4$) [30]. When experimental conditions such as the cation itself (Na^+, K^+ and divalent cations) [12,31,32], the cation concentration [30,33,34], the DNA concentration [27,30], crowding agents (addition of polyethylene glycol to mimic molecular crowding in cells) [20] or the temperature [35,36] are changed, alterations of the G-quadruplex structure are expected [9]. Recently, it has been demonstrated that specific telomeric DNA sequences can be exploited in sensing because, e.g., the RevHumTel sequence formation of G-quadruplexes is highly ion-specific when connected to DNA nanostructures [30,36]. In this line, Noer et al. studied the folding dynamics and conformational heterogeneity exhibited by human telomeric G-quadruplex structures in the presence of Na^+ ions by single-molecule FRET microscopy [37]. Therefore, in the present work, we took the time to analyze the influence of different salts of monovalent and divalent cations on the specific G-quadruplex structure and conformation of the reversed human telomeric DNA (RevHumTel, 5′-TT (GGG ATT)$_4$) using CD spectroscopy and the principle of Förster resonance energy transfer (FRET). For this, we compare our measured CD spectra with previously published CD spectra of related G-quadruplex structures to comment on the different conformation of the G-quadruplex structure. To further support the CD spectroscopy results, FRET measurements were additionally performed to determine the distance between the 5′- and 3′-end (when modified with donor and acceptor molecules) and deduce the specific G-quadruplex structures [22,24,35]. Therefore, we considered the folding of unmodified RevHumTel in the presence of KCl, NaCl, $MgCl_2$ and $CaCl_2$ (0–500 mM). For the FRET experiments, the telomeric DNA has been modified with Cyanine3 (Cy3) at its 5′-end and with Fluorescein (FAM) at its 3′-end (5′-Cy3-TT (GGG ATT)$_4$-FAM). Here, FAM acts as the FRET donor and Cy3 as the FRET acceptor. By combining the findings of CD spectroscopy and FRET experiments, we are able to estimate the specific G-quadruplex structure formed from RevHumTel in presence of different salts.

2. Results and Discussion

2.1. CD Spectroscopy

The CD spectra for RevHumTel (c = 8.6 μM, diluted in TAE buffer (1x)) for the different salts are shown in Figure 1. Different salts lead to different CD spectra. The telomeric DNA in a pure buffer (TAE 1x) gives rise to a negative peak at 240 nm and two positive peaks at 255 nm and 280 nm. The TAE buffer does not influence the CD spectra compared to the free telomeric DNA in ultra-pure water, as shown in the SI Figure S2. The CD spectrum changes when KCl is added to the solution (Figure 1A). After the addition of ca. 10 mM KCl, an intense positive peak at 288 nm with a shoulder at 275 nm becomes visible indicating the G-quadruplex formation. A broad negative CD band at (240–250) nm is also visible. Please note that the shape of the CD spectrum does not change significantly with an increasing amount of KCl, meaning that the salt concentration does not influence the specific G-quadruplex structure. Only the intensity of the CD bands rises with an increasing KCl concentration showing that the fraction of folded G-quadruplex structures increases. By comparing with CD spectra found in literature, the present CD spectra indicate the formation of a "hybrid-type" G-quadruplex structure by RevHumTel in presence of KCl [16].

The CD spectra after the NaCl addition (Figure 1B) look different compared to the CD spectra in the presence of KCl. More NaCl is needed to induce a change in the CD spectra, meaning that the G-quadruplex folds at higher NaCl concentrations (ca. 200 mM) compared to KCl (ca. 10 mM). This can be attributed to two different association constants in presence of KCl and NaCl (the association constant of KCl is higher compared to NaCl) [36]. Furthermore, the shape of the CD spectra after the G-quadruplex formation is

rather different. In the presence of NaCl, the CD spectra have a minimum of 235 nm (not negative values) and two intense positive peaks at 270 nm and 290 nm. Again, the salt concentration does not influence the shape of the CD spectrum. Hence, the G-quadruplex structure is not dependent on the salt concentration. By comparing this CD spectrum with the previously reported CD spectra, the CD spectrum could be attributed to a "hybrid-type" or a mixture of parallel and anti-parallel G-quadruplexes [16].

It is not only the monovalent cations that can induce the formation of G-quadruplex structures. Divalent cations such as Mg^{2+} and Ca^{2+} are also known to stabilize G-quadruplexes [32,38,39], which is particularly important for G-quadruplexes connected to Mg^{2+}-stabilized DNA nanostructures [30,36,40]. For $MgCl_2$, the CD spectra are shown in Figure 1C. Here, the CD spectra can be clearly associated with a parallel G-quadruplex structure [15,16,19–23]. In presence of $MgCl_2$, two intense signals are present (positive peak at (240–245) nm and negative peak at 265 nm). The concentration of $MgCl_2$ needed for G-quadruplex formation is as low as 2 mM. Again, the shape of the CD spectra is almost unaffected by the salt concentration (which also accords with the concentration used in previous studies) [41,42] meaning that the G-quadruplex structure is also unaffected by the salt concentration [16].

The CD spectra for $CaCl_2$ addition are shown in Figure 1D. Again, the CD spectrum changes at a salt concentration of 2 mM, meaning that the G-quadruplex structure folds at low $CaCl_2$ concentrations. After the $CaCl_2$ addition, a positive peak at 265 nm and a negative peak at 242 nm appears. This can also be attributed to a parallel G-quadruplex structure [15,16,19–23]. Please note that at high salt concentrations (500 mM), the peak at 265 nm decreases, which could indicate a partial destabilization of the G-quadruplex, which could occur by the accumulation of excess counterions in the vicinity of the G-quadruplex structure [43].

Finally, we have recorded CD spectra of RevHumTel in the presence of a mixture of ions corresponding to physiological conditions (i.e., 143 mM Na^+, 5 mM K^+, 2,5 mM Ca^{2+}, 1 mM Mg^{2+}, Figure S3). The CD spectrum shows a negative dip in the range 240–250 nm and a positive peak at around 290 nm with a shoulder at 270 nm indicating that in the mixture of salts under physiological conditions K^+ ions dominate the formation of G-quadruplex structures, i.e., a hybrid-type G-quadruplex structure is formed. This is in line with melting curves measured by UV absorption at a concentration of 200 mM of each salt indicating the highest melting points for K^+ induced G quadruplexes showing two melting stages (50 °C and 80 °C, Figure S5), whereas Na^+ induced G-quadruplexes show the lowest melting point (23 °C).

2.2. FRET Experiments

To verify the findings of the CD spectroscopy, especially for ambiguous spectra we performed FRET experiments at constant salt concentrations to determine the 5′-3′-end distances (5′-end: Cy3, 3′-end: FAM). Please note that $MgCl_2$ and $CaCl_2$ are able to quench fluorescence at high concentrations. This could be attributed to dynamic quenching experienced by donor-acceptor dye pair(s) induced by divalent ions at higher concentrations [44]. Hence, measurements have been performed at concentrations as low as 30 mM and 2 mM, respectively. For KCl, the concentration has been set to 195 mM and for NaCl it has been set to 490 mM to assure a complete folding. The FRET efficiency [45,46]. *E* depends on the donor-acceptor distance *R* and behaves according to the following Equation (1),

$$E = \frac{R_0^6}{R_0^6 + R^6} \tag{1}$$

with R_0 being the Förster distance. The Förster distance is the distance at which the FRET efficiency is equal to 50 % (FRET and donor fluorescence are equally probable). The Förster distance is a FRET-pair-specific parameter and can be determined as followed.

$$R_0^6 = \frac{9 \ln 10 \kappa^2 \phi_D J(\lambda)}{128 \pi^5 n^4 N_{AV}} \tag{2}$$

Here, κ^2 is the dipole orientation factor, ϕ_D the donor's quantum yield, n is the refractive index of the surrounding media, N_{AV} is Avogadro's number and $J(\lambda)$ is the overlap integral which represents the spectral overlap between the donor's emission spectrum and the acceptor's absorption spectrum (Figure S6). The spectral overlap integral is as follows,

$$J(\lambda) = \frac{\int F_D(\lambda) \epsilon_A(\lambda) \lambda^4 d\lambda}{\int F_D(\lambda) d\lambda} \tag{3}$$

where λ is the wavelength, $F_D(\lambda)$ is the donor's emission spectrum and $\epsilon_A(\lambda)$ is the acceptor's extinction coefficient spectrum. The Förster distance for FAM and Cy3 has been found to be 6.7 nm (see SI). The FRET efficiency has been determined based on the donor's fluorescence decay time as follows,

$$E = 1 - \frac{\tau_{DA}}{\tau_D} \tag{4}$$

with τ_{DA} being the donor's fluorescence decay time in presence of the acceptor and τ_D the fluorescence decay time in absence of the acceptor molecule (τ_D = 4.3 ns). The FAM fluorescence decay curves in presence of different salts have been measured using time-correlated single photon counting (TCSPC, see experimental section) and have been fitted tri-exponentially (three different decay time components, each decay time component corresponds to τ_{DA}). Each decay time component can be attributed to a certain donor-acceptor distance. The FAM-Cy3 distances can be determined based on Equation (5) [47,48].

$$R = R_0 \sqrt[6]{\frac{1}{E} - 1} \tag{5}$$

Based on the experimental FAM-Cy3-distances (corresponding to 5′-3′-distances) certain G-quadruplex structures can be assigned in presence of different salts. An overview of possible 5′-3′-distances in different G-quadruplex structures is shown in Scheme 1. The 5′-3′-end can be at distances of approximately 4.1 nm, 5.8 nm, 4.6 nm or 6.1 nm (a linker length of 0.7 nm between fluorophore and DNA has been considered) depending on the position of 5′- or 3′-end in the G-quadruplex resulting from the specific loop and strand orientations [12,13].

In the presence of KCl, three different decay time components have been found with $\tau_{DA,1}$ = 0.24 ns, $\tau_{DA,2}$ = 0.66 ns, $\tau_{DA,3}$ = 4.01 ns (fluorescence decay curve in presence of KCl is shown in Figure 2A). The third decay time component corresponds to a distance of 10.4 nm which can be attributed to the unfolded G-quadruplex (R (FAM-Cy3) = 26 nb ≈ 8.6 nm, when determined based on the structural properties of double-stranded DNA) [49]. The first and second decay time components correspond to distances of 4.2 nm and 5.0 nm, respectively, and can be ascribed to two different G-quadruplex structures. For a distance of 4.2 nm, a G-quadruplex structure, where the 5′- and 3′-end are located next to each other on the same G-tetrad (Scheme 1 red), can be assigned (nominal distance of 4.1 nm). A distance of 5.0 nm can be ascribed to a G-quadruplex where the 5′- and 3′-end are located on different G-tetrads and on the same side of the G-quadruplex oriented diagonally to each other (nominal distance 4.6 nm; see Scheme 1 green). This is in tandem with the CD results obtained in Figure 1A, which indicates the "hybrid-type" G-quadruplex structure.
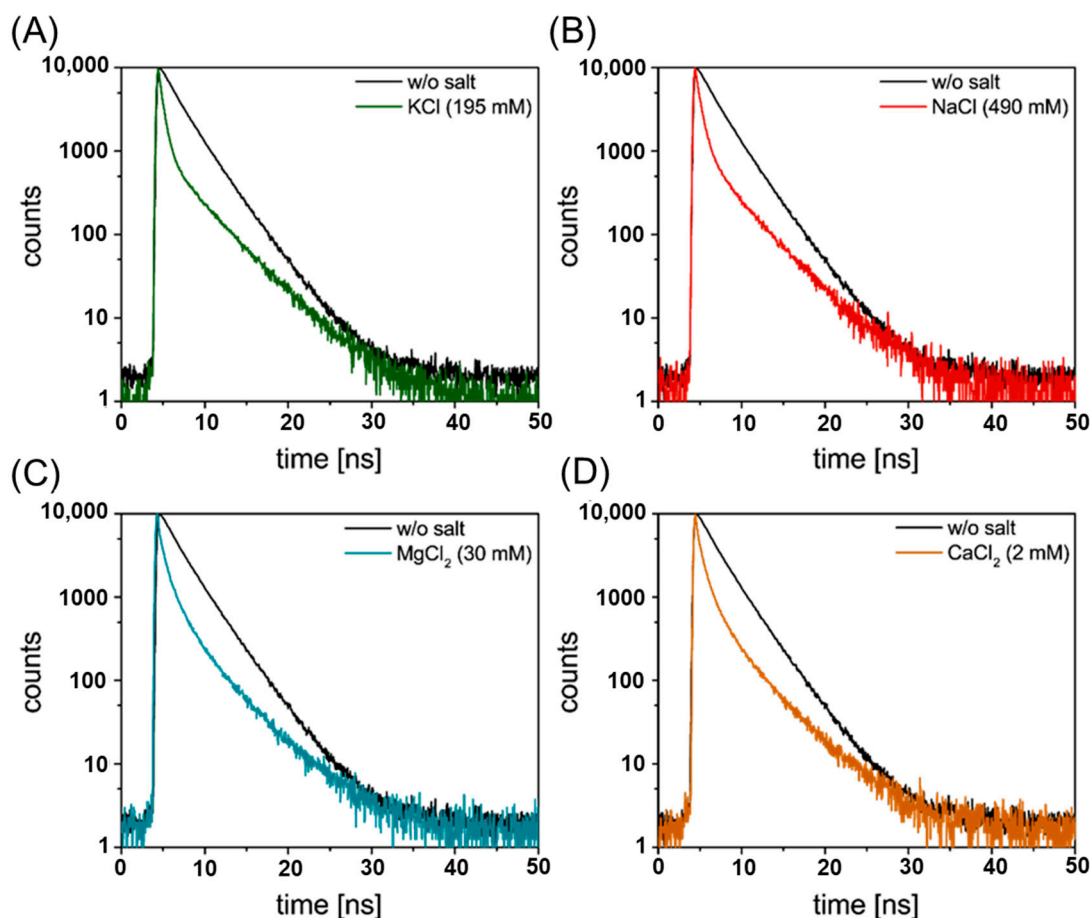
Figure 2. FAM fluorescence decay curves (c(DNA) = 5 nM, λ_{ex} = 490 nm, λ_{em} = 520 nm) for RevHum-Tel in presence of different salts (**A**) KCl (c = 195 mM), (**B**) NaCl (c = 490 nm), (**C**) MgCl$_2$ (c = 30 mM) and (**D**) CaCl$_2$ (c = 2 mM). The fluorescence decay curves have been fitted tri-exponentially to determine different FAM-Cy3 distances (5′-3′-end distances) which help identify different G-quadruplex structures in presence of different salts.

For NaCl, the following decay time components have been found: $\tau_{DA,1}$ = 0.27 ns, $\tau_{DA,2}$ = 0.78 ns and $\tau_{DA,3}$ = 3.94 ns. The FAM fluorescence decay curve in presence of NaCl is shown in Figure 2B. These decay time components correspond to the following distances R_1 = 4.3 nm, R_2 = 5.2 nm and R_3 = 10 nm, respectively. Again, the distance based on the third decay time component belongs to the unfolded G-quadruplex structure. A distance of 4.3 nm can be attributed to a G-quadruplex structure where the 5′- and 3′-end are located next to each other on the same G-tetrad (Scheme 1, red) and can be assigned to "chair-type" (nominal distance of 4.1 nm) or it could be that the 5′- and 3′-end are located on different G-tetrads and on the same side of the G-quadruplex structure oriented diagonally to each other (theoretical distance: 4.6 nm calculated considering the spacer distance of 0.7 nm between the fluorophore and DNA base sequence, see Figure 1 green). On the other hand, when the 5′- end 3′-end are located on the same G-tetrad and are oriented diagonally to each other (different side of the G-quadruplex, see Figure 1 yellow) a distance of 5.8 nm is expected which corresponds well with the determined distance of 5.2 nm. This indicates the formation of a "hybrid-type" or a mixture of parallel and anti-parallel G-quadruplexes supported by CD analysis.

The FAM fluorescence decay curves in presence of MgCl$_2$ are depicted in Figure 2C. With a tri-exponential fit the fluorescence decay time components have been found to be $\tau_{DA,1}$ = 0.24 ns, $\tau_{DA,2}$ = 1.07 ns, $\tau_{DA,3}$ = 3.78 ns. The third decay component corresponds to a distance of 9.3 nm which can be assigned to the unfolded G-quadruplex. For the first decay time component, a distance of 4.2 nm has been determined which can be ascribed to

a G-quadruplex structure where the 5'- and 3'-end are located on different G-tetrads and oriented diagonally to each other (expected distance: 4.6 nm, Scheme 1 green). The second decay time component corresponds to a distance of 5.6 nm which—along with the CD results discussed below—can be assigned to a G-quadruplex structure where the 5'- and 3'-end are located on different G-tetrads and oriented diagonally to each other (different sides of the G-quadruplex, nominal distance: 6.0 nm, Scheme 1 blue) termed as new-hybrid.

For $CaCl_2$ addition, similar values compared to $MgCl_2$ addition have been found. The FAM fluorescence decay curves in presence of $CaCl_2$ are shown in Figure 2D. The third decay time component ($\tau_{DA,3}$ = 3.80 ns) corresponds to a distance of 9.4 nm which belongs to the unfolded G-quadruplex structure. A distance of 4.1 nm has been determined for the first decay time component ($\tau_{DA,1}$ = 0.24 ns). Again, this can be ascribed to a G-quadruplex structure where the 5'- and 3'-end are located on different G-tetrads and oriented diagonally to each other (expected distance: 4.6 nm, Scheme 1 green). Finally, a distance of 5.5 nm ($\tau_{DA,2}$ = 1.07 ns) can be attributed to a G-quadruplex structure where the 5'- and 3'-end are located on different G-tetrads and oriented diagonally to each other (theoretical distance: 6.0 nm, Scheme 1 blue) which we assign as new-hybrid structure. The above assignment for $MgCl_2$ and $CaCl_2$ holds true based on the results from CD spectra which indicate the parallel conformation of the structure.

3. Methods and Materials

3.1. Materials and Chemicals

The telomeric DNA strands (RevHumTel and HumTel), unmodified and modified with organic dyes, have been acquired from Metabion International AG (Planegg, Germany) (HPLC purified, dissolved in water). All DNA strands have been used as delivered without further treatment. Magnesium chloride ($MgCl_2$, ≥98 %), sodium chloride (NaCl) and Tris acetate-EDTA buffer (TAE buffer, 10× concentrated) have been acquired from Sigma Aldrich (Hamburg, Germany). The diluted TAE buffer (1× concentrated, in ultrapure water (Merck KGaA, Darmstadt, Germany)) (pH = 8.2) contains 40 mM Tris-acetate and 1 mM EDTA. Calcium chloride ($CaCl_2$, ≥98 %) has been purchased from Carl Roth (Karlsruhe, Germany) and potassium chloride (KCl) from VWR Prolabo (Darmstadt, Germany). The salt solutions have been prepared in ultrapure Millipore water.

3.2. CD Spectroscopy

CD spectroscopy has been performed on a JASCO J-815 CD spectrometer (JASCO Labor- und Datentechnik GmbH, Pfungstadt, Germany) with 1 mm quartz cuvettes from Hellma Analytics. For this, the DNA strands (unmodified RevHumTel (5'-TT (GGG ATT)$_4$) and HumTel (5'-TT (GGG TTA)$_3$ GGG TTT), c = 100 μM) have been diluted in TAE buffer (1× concentrated, incl. the respective salt concentration indicated below) to a final DNA concentration of 8.6 μM. KCl, NaCl, $MgCl_2$ or $CaCl_2$ (c = 200 mM, 2 M) have been used to induce the G-quadruplex formation (incubation for 15 min at room temperature, Figure S4 shows that annealing at 40 °C yields the same result). Each sample has been prepared separately for each salt concentration ranging from 0 to 500 mM (c = (2, 10, 20, 200, 500) mM). The pure TAE buffer has been measured individually and subtracted from the sample's CD spectrum. For the CD experiment of an unmodified RevHumTel DNA strand in the presence of a mixture of four different salts corresponding to physiological conditions (Na^+: 143 mM; K^+: 5 mM; Ca^{2+}: 2.5 mM; Mg^{2+}: 1 mM), a final concentration of 8.6 μL in 1X TAE is maintained. A blank buffer was prepared for each reaction, measured and subtracted from the sample CD spectrum. The CD spectra have been recorded from 200 to 320 nm with the following settings: digital integration time: 4 s, sensitivity: standard, spectral bandwidth: 1 nm, data pitch: 1 nm, start mode: immediately, scanning mode: continuous, scanning speed: 50 nm/min, accumulation: 3.

3.3. Melting Curves

The RevHumTel DNA diluted in 1X TAE buffer, with the final concentration of 3 µM, is considered. Four different batches of four different cations (KCl, NaCl, MgCl$_2$, CaCl$_2$) with a final concentration of 200 mM each are prepared. The melting temperature analysis has been recorded on a SPECORD 200 UV/Vis spectrometer (Analytik Jena AG, Jena, Germany) in a standard quartz cuvette. The temperature of the cell holder was increased from 4 °C to 90 °C at a rate of 1 °C/min (integration time: 0.1 s) and the UV-absorbance is collected from 250 to 320 nm.

3.4. Time-Correlated Single Photon Counting

For time-correlated single photon counting (TCSPC) measurements, the DNA (RevHumTel modified with FAM and Cy3, 5′-Cy3-TT (GGG ATT)$_4$-FAM, c = 100 µM) has been diluted in a TAE (1×) buffer to a concentration of 5 nM. After the addition of salts to induce the G-quadruplex formation (KCl (c = 195 mM), NaCl (c = 490 mM), MgCl$_2$ (c = 30 mM) and CaCl$_2$ (c = 2 mM)) the samples have been incubated for 15 min at room temperature and measured afterwards. TCSPC measurements have been performed on a FLS920 fluorescence spectrophotometer from Edinburgh Instruments Ltd. with the F900 software (Edinburgh Instruments Ltd, Livingston, UK.) using 3 mm quartz cuvettes (Hellma Analytics). The samples have been measured in a 90° setup. As an excitation source, a supercontinuum white light source SC-400-PP from Fianium/NKT Photonics A/S (0.5–20 MHz, 400 nm < λ < 24,000 nm, pulse width: ca. 30 ps) and, as a detector, a multi-channel-plate ELDY EM1-132/300 from Europhoton GmbH have been used. The excitation wavelength has been set to (490 ± 1) nm and the emission wavelength to (520 ± 1) nm. The fluorescence decay curves (intensity-time-function $I(t)$) have been fitted with tri-exponential functions (Equation (6)) depending on the sample using the FAST software (Edinburgh Instruments, Livingston, UK).

$$I(t) = \sum_{i=1}^{n} A_i e^{-\frac{t}{\tau_i}} \tag{6}$$

Here, τ_i is the decay time component and A_i is the amplitude characteristic for each decay time component.

4. Conclusions

After analyzing the CD spectra and fluorescence decay curves of RevHumTel in the presence of different salts, we can predict the specific G-quadruplex structures which are folded in different environments. Please note that the donor-acceptor-distances determined in this work are error prone. Since the value for R_0 depends on a variety of parameters and not all of them are easily accessible (e.g., κ^2), the R_0 calculated here are not necessarily exact. Nevertheless, by combining CD spectroscopy with FRET measurements we can get closer insights into the most probable G-quadruplex structures formed in the presence of different salts. Based on the CD spectra the strand and loop orientations are accessible while the FRET experiments yield the locations of 5′- and 3′-end in the G-quadruplex. Furthermore, based on the FRET measurements it is evident that at least two different G-quadruplex structures are present for all salts. The different possible G-quadruplex structures are shown in Figure 3. As discussed above the CD spectrum in presence of KCl indicates the formation of a "hybrid-type" G-quadruplex structure which is also confirmed by a 5′-3′-distance of 5.0 nm (Figure 3A, right). A distance of 4.2 nm can be ascribed to an anti-parallel "chair-type" G-quadruplex structure (Figure 3A, left) which can also be confirmed in the CD spectrum (positive peak at 288 nm, negative peak at 240 nm). For NaCl, the CD spectrum is relatively ambiguous ("hybrid-type" or mixture of parallel/anti-parallel G-quadruplex structures). Together with the FRET experiments three different G-quadruplex structures in presence of NaCl are conceivable. A 5′-3′-distance of 5.2 nm can be attributed to an anti-parallel G-quadruplex structure ("basket-type", Figure 3B, right). A distance of 4.3 nm could be an indication of an antiparallel chair-type conformation (Figure 3A, left), the for-

mation of a parallel G-quadruplex structure ("propeller-type", Figure 3B, left) or a "hybrid-type" G-quadruplex (two lateral and one external loop, Figure 3B, middle). For $MgCl_2$ and $CaCl_2$, the CD spectra indicate the formation of the same G-quadruplex structures which can also be confirmed by FRET measurements (determination of similar distances, R_1 = 4.2 nm/4.1 nm, R_2 = 5.6 nm/5.5 nm). Furthermore, the CD spectra indicate the formation of only parallel G-quadruplex structures (the distance of 4.2 nm/4.1 nm has to belong to a G-quadruplex where the 5'- and 3'-end are located on different G-tetrads and oriented diagonally to each other). Since two different distances in the FRET experiments have been found for the folded G-quadruplex structure the parallel G-quadruplex structures are based on different strand routings as shown in Figure 3C, D for $MgCl_2$ and $CaCl_2$, respectively. The G-quadruplex structures and conformation attained by RevHumTel in presence of different salts has been summarized in Table 1 based on theoretical and experimental results obtained in this study. In future research, the combination of FRET and CD measurements could be used to explore the folding of other G quadruplex structures and the method can be extended to other biologically relevant ions.
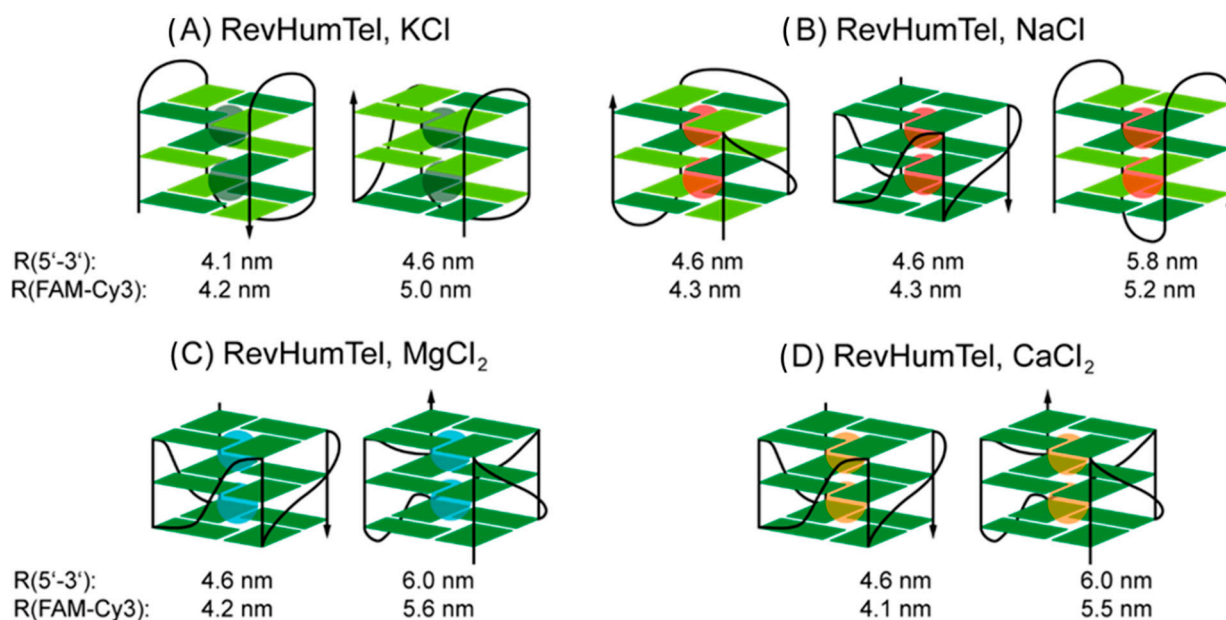

Figure 3. G-quadruplex structures for RevHumTel in presence of different salts (**A**) KCl, (**B**) NaCl, (**C**) $MgCl_2$ and (**D**) $CaCl_2$. The G-quadruplex structures have been determined based on CD spectroscopy and FRET measurements. Dark green rectangles represent antiglycosidic angles for G and light green syn orientation.

Table 1. Summary of G-quadruplex structures and conformation attained by RevHumTel in presence of different salts based on the theoretical and experimental values obtained from FRET and CD results as tabulated below.

Structure	Conformation	FRET Distance	Salt	Conformation from Circular Dichroism (CD)	Experimental FRET Distance	Structural Assignment
Theoretical Value			**Experimental Values**			
Chair	anti-parallel	4.1	KCl	hybrid	4.2/5.0	Hybrid + chair
Basket	anti-parallel	5.8	NaCl	hybrid/parallel + anti-parallel	4.2/5.2	Hybrid + basket
Propeller	parallel	4.6	$MgCl_2$	parallel	4.2/5.6	Propeller + new hybrid
Hybrid	anti-parallel + parallel	4.6	$CaCl_2$	parallel	4.1/5.5	Propeller + new hybrid
New hybrid	anti-parallel + parallel	6.0				

References

1. Dolinnaya, N.G.; Ogloblina, A.M.; Yakubovskaya, M.G. Structure, properties, and biological relevance of the DNA and RNA G-quadruplexes: Overview 50 years after their discove ry. *Biochemistry* **2016**, *81*, 1602–1649. [CrossRef]
2. Neidle, S.; Parkinson, G.N. The structure of telomeric DNA. *Curr. Opin. Struct. Biol.* **2003**, *13*, 275–283. [CrossRef]
3. Choi, J.; Majima, T. Conformational changes of non-B DNA. *Chem. Soc. Rev.* **2011**, *40*, 5893–5909. [CrossRef] [PubMed]
4. Burge, S.; Parkinson, G.N.; Hazel, P.; Todd, A.K.; Neidle, S. Quadruplex DNA: Sequence, topology and structure. *Nucleic Acids Res.* **2006**, *34*, 5402–5415. [CrossRef] [PubMed]
5. Blackburn, E.H. The molecular structure of centromeres and telomeres. *Annu. Rev. Biochem.* **1984**, *53*, 163–194. [CrossRef]
6. Sundquist, W.I.; Klug, A. Telomeric DNA dimerizes by formation of guanine tetrads between hairpin loops. *Nature* **1989**, *342*, 825–829. [CrossRef]
7. Huppert, J.L. Hunting G-quadruplexes. *Biochimie* **2008**, *90*, 1140–1148. [CrossRef]
8. Bang, I. Untersuchungen über die Guanylsäure. *Biochem. Z.* **1910**, *26*, 293–311.
9. Neidle, S. *Therapeutic Applications of Quadruplex Nucleic Acids*, 1st ed.; Elsevier/Academic Press: London, UK; Waltham, MA, USA; San Diego, CA, USA, 2012.
10. Neidle, S.; Balasubramanian, S. *Quadruplex Nucleic Acids*; RSC Publishing: Cambridge, UK, 2006.
11. Kogut, M.; Kleist, C.; Czub, J. Molecular dynamics simulations reveal the balance of forces governing the formation of a guanine tetrad—A common structural unit of G-quadruplex DNA. *Nucleic Acids Res.* **2016**, *44*, 3020–3030. [CrossRef]
12. Parkinson, G.N.; Lee MP, H.; Neidle, S. Crystal structure of parallel quadruplexes from human telomeric DNA. *Nature* **2002**, *417*, 876–880. [CrossRef]
13. Wang, Y.; Patel, D.J. Solution structure of the human telomeric repeat d[AG3(T2AG3)3] G-tetraplex. *Structure* **1993**, *1*, 263–282. [CrossRef]
14. Kelly, S.M.; Jess, T.J.; Price, N.C. How to study proteins by circular dichroism. *Biochim. Et Biophys. Acta* **2005**, *1751*, 119–139. [CrossRef] [PubMed]
15. Holm AI, S.; Kohler, B.; Hoffmann, S.V.; Brøndsted Nielsen, S. Synchrotron radiation circular dichroism of various G-quadruplex structures. *Biopolymers* **2010**, *93*, 429–433. [CrossRef]
16. Karsisiotis, A.I.; Hessari, N.M.; Novellino, E.; Spada, G.P.; Randazzo, A.; Silva MW, D. Topological characterization of nucleic acid G-quadruplexes by UV absorption and circular dichroism. *Angew. Chem. Int. Ed.* **2011**, *50*, 10645–10648. [CrossRef] [PubMed]
17. Gray, D.M.; Wen, J.-D.; Gray, C.W.; Repges, R.; Repges, C.; Raabe, G.; Fleischhauer, J. Measured and calculated CD spectra of G-quartets stacked with the same or opposite polarities. *Chirality* **2008**, *20*, 431–440. [CrossRef]
18. Kypr, J.; Kejnovska, I.; Renciuk, D.; Vorlickova, M. Circular dichroism and conformational polymorphism of DNA. *Nucleic Acids Res.* **2009**, *37*, 1713–1725. [CrossRef] [PubMed]
19. Marušič, M.; Plavec, J. The Effect of DNA Sequence Directionality on G-Quadruplex Folding. *Angew. Chem. Int. Ed.* **2015**, *54*, 11716–11719. [CrossRef] [PubMed]
20. Heddi, B.; Phan, A.T. Structure of human telomeric DNA in crowded solution. *J. Am. Chem. Soc.* **2011**, *133*, 9824–9833. [CrossRef] [PubMed]
21. Balagurumoorthy, P.; Brahmachari, S.K.; Mohanty, D.; Bansal, M.; Sasisekharan, V. Hairpin and parallel quartet structures for telomeric sequences. *Nucleic Acids Res.* **1992**, *20*, 4061–4067. [CrossRef]
22. Gray, R.D.; Trent, J.O.; Chaires, J.B. Folding and unfolding pathways of the human telomeric G-quadruplex. *J. Mol. Biol.* **2014**, *426*, 1629–1650. [CrossRef]

23. Gattuso, H.; Spinello, A.; Terenzi, A.; Assfeld, X.; Barone, G.; Monari, A. Circular Dichroism of DNA G-Quadruplexes: Combining Modeling and Spectroscopy To Unravel Complex Structures. *J. Phys. Chem. B* **2016**, *120*, 3113–3121. [CrossRef]
24. Tippana, R.; Xiao, W.; Myong, S. G-quadruplex conformation and dynamics are determined by loop length and sequence. *Nucleic Acids Res.* **2014**, *42*, 8106–8114. [CrossRef]
25. Li, J.; Correia, J.J.; Wang, L.; Trent, J.O.; Chaires, J.B. Not so crystal clear: The structure of the human telomere G-quadruplex in solution differs from that present in a crystal. *Nucleic Acids Res.* **2005**, *33*, 4649–4659. [CrossRef]
26. Phan, A.T. Human telomeric G-quadruplex: Structures of DNA and RNA sequences. *FEBS J.* **2010**, *277*, 1107–1117. [CrossRef]
27. Renciuk, D.; Kejnovska, I.; Skolakova, P.; Bednarova, K.; Motlova, J.; Vorlickova, M. Arrangements of human telomere DNA quadruplex in physiologically relevant K+ solutions. *Nucleic Acids Res.* **2009**, *37*, 6625–6634. [CrossRef]
28. Marchand, A.; Gabelica, V. Folding and misfolding pathways of G-quadruplex DNA. *Nucleic Acids Res.* **2016**, *44*, 10999–11012. [CrossRef]
29. Kaushik, M.; Bansal, A.; Saxena, S.; Kukreti, S. Possibility of an antiparallel (tetramer) quadruplex exhibited by the double repeat of the human telomere. *Biochemistry* **2007**, *46*, 7119–7131. [CrossRef]
30. Olejko, L.; Cywinski, P.J.; Bald, I. An ion-controlled four-color fluorescent telomeric switch on DNA origami structures. *Nanoscale* **2016**, *8*, 10339–10347. [CrossRef]
31. Ambrus, A.; Chen, D.; Dai, J.; Bialis, T.; Jones, R.A.; Yang, D. Human telomeric sequence forms a hybrid-type intramolecular G-quadruplex structure with mixed parallel/antiparallel strands in potassium solution. *Nucleic Acids Res.* **2006**, *34*, 2723–2735. [CrossRef]
32. Miyoshi, D.; Nakao, A.; Toda, T.; Sugimoto, N. Effect of divalent cations on antiparallel G-quartet structure of d(G4T4G4). *FEBS Lett.* **2001**, *496*, 128–133. [CrossRef]
33. Palacký, J.; Vorlíčková, M.; Kejnovská, I.; Mojzeš, P. Polymorphism of human telomeric quadruplex structure controlled by DNA concentration: A Raman study. *Nucleic Acids Res.* **2013**, *41*, 1005–1016. [CrossRef]
34. Largy, E.; Marchand, A.; Amrane, S.; Gabelica, V.; Mergny, J.-L. Quadruplex Turncoats: Cation-Dependent Folding and Stability of Quadruplex-DNA Double Switches. *J. Am. Chem. Soc.* **2016**, *138*, 2780–2792. [CrossRef]
35. Lee, J.Y.; Okumus, B.; Kim, D.S.; Ha, T. Extreme conformational diversity in human telomeric DNA. *Proc. Natl. Acad. Sci. USA* **2005**, *102*, 18938–18943. [CrossRef]
36. Olejko, L.; Cywinski, P.J.; Bald, I. Ion-selective formation of a guanine quadruplex on DNA origami structures. *Angew. Chem. Int. Ed.* **2015**, *54*, 673–677. [CrossRef]
37. Noer, S.L.; Preus, S.; Gudnason, D.; Aznauryan, M.; Mergny, J.-L.; Birkedal, V. Folding dynamics and conformational heterogeneity of human telomeric G-quadruplex structures in Na+ solutions by single molecule FRET microscopy. *Nucleic Acids Res.* **2016**, *44*, 464–471. [CrossRef] [PubMed]
38. Miyoshi, D.; Inoue, M.; Sugimoto, N. DNA logic gates based on structural polymorphism of telomere DNA molecules responding to chemical input signals. *Angew. Chem. Int. Ed.* **2006**, *45*, 7716–7719. [CrossRef] [PubMed]
39. Ruttkay-Nedecky, B.; Kudr, J.; Nejdl, L.; Maskova, D.; Kizek, R.; Adam, V. G-quadruplexes as sensing probes. *Molecules* **2013**, *18*, 14760–14779. [CrossRef]
40. Rackwitz, J.; Bald, I. Low-Energy Electron-Induced Strand Breaks in Telomere-Derived DNA Sequences-Influence of DNA Sequence and Topology. *Chem. A Eur. J.* **2018**, *24*, 4680–4688. [CrossRef] [PubMed]
41. Jiang, H.-X.; Cui, Y.; Zhao, T.; Fu, H.-W.; Koirala, D.; Punnoose, J.A.; Kong, D.-M.; Mao, H. Divalent cations and molecular crowding buffers stabilize G-triplex at physiologically relevant temperatures. *Sci. Rep.* **2015**, *5*, 9255. [CrossRef]
42. Pal, S.; Paul, S. Theoretical investigation of conformational deviation of the human parallel telomeric G-quadruplex DNA in the presence of different salt concentrations and temperatures under confinement. *Phys. Chem. Chem. Phys.* **2021**, *23*, 14372–14382. [CrossRef] [PubMed]
43. Kim, B.G.; Evans, H.M.; Dubins, D.N.; Chalikian, T.V. Effects of Salt on the Stability of a G-Quadruplex from the Human c-MYC Promoter. *Biochemistry* **2015**, *54*, 3420–3430. [CrossRef] [PubMed]
44. Adenier, A.; Aaron, J.J. A spectroscopic study of the fluorescence quenching interactions between biomedically important salts and the fluorescent probe merocyanine 540. *Spectrochim. Acta A Mol. Biomol. Spectrosc.* **2002**, *58*, 543–551. [CrossRef]
45. Förster, T. Energiewanderung und Fluoreszenz. *Naturwissenschaften* **1946**, *33*, 166–175. [CrossRef]
46. Förster, T. Zwischenmolekulare Energiewanderung und Fluoreszenz. *Ann. Phys.* **1948**, *437*, 55–75. [CrossRef]
47. Lakowicz, J.R. *Principles of Fluorescence Spectroscopy*, 3rd ed.; Springer: New York, NY, USA, 2006.
48. Valeur, B.; Berberan-Santos, M.N. *Molecular Fluorescence: Principles and Applications*, 2nd ed.; Wiley-VCH: Weinheim, Germany, 2013.
49. Berg, J.M.; Stryer, L.; Tymoczko, J.L. *Biochemie*, 7th ed.; Springer Spektrum: Berlin, Germany, 2013.